Electronic Supplementary Information (ESI)

Capacitive deionization of saline water using graphene nanospheres decorated N-doped layered mesoporous carbon frameworks

*Zaheen Ullah Khan, Tingting Yan, Jinlong Han, Liyi Shi and Dengsong Zhang**

Department of Chemistry, Research Center of Nano Science and Technology, State Key Laboratory of Advanced Special Steel, School of Materials Science and Engineering, Shanghai University, Shanghai, 200444, China

*Corresponding Author

E-mail: dszhang@shu.edu.cn; Tel: +86-21-66137152.

Physical characterization

The morphology of the all carbon samples were characterized by using transmission electron microscopy (TEM, JEOL JEM-200CX) and field emission scanning electron microscopy (SEM, JEOL JEM-700F). High-resolution transmission electron microscopy (HR-TEM) images were observed by using JEOL JEM-2010F. X-ray diffraction (XRD) was tested on Rigaku D/MAX-RB X-ray diffractometer using crystal monochromatic Cu Kα radiation. X-ray photoelectron spectroscopy (XPS) data was detected on a Perkin-Elmer PHI 5000C ESCA system equipped with a dual anode Mg Ka (1253.6 eV) X-ray source. Specific surface area and macro and mesopore size distribution was calculated by using Brunauer-Emmett-Teller (BET) with a Micromeritics ASAP 2010 analyzer and Barrett-Joyner-Halenda (BJH) model. The volume of micropores and the pore size distribution (PSD) were measured by using the density functional theory (DFT) method. The volume of mesopores was determined by subtracting the micropores volume from the total pore volume of N2 adsorbed. Raman spectra were carried out on Raman spectrometer (JY H800UV) (INVIA). The surface wettability of the samples was calculated by dynamic water contact angle analysis by using (Krüss DSA100). A 1μL drop of water with a rate of $1\mu Ls^{-1}$ was placed on the surface of electrode and series of images were taken as function of contact time.

Electrochemical characterization

The galvanostatic charge-discharge (GCD), cyclic voltammetry (CV) and electrochemical impedance spectroscopy (EIS) were performed in 0.5 mol L^{-1} NaCl salt solutions by using three-electrode cell system that consisted of working electrode, graphite electrode and calomel reference electrode. The working electrodes were fabricated by mixing polytetrafluoroethylene (10%) sample and material (90%) in ethanol to make homogenous pastes. The slurry was pressed on sheet of graphite and then dried at 110 ^{o}C overnight. The frequency range for EIS was 10 mHz to10 kHz and the amplitude of the applied voltage was 5 mV for all electrodes.

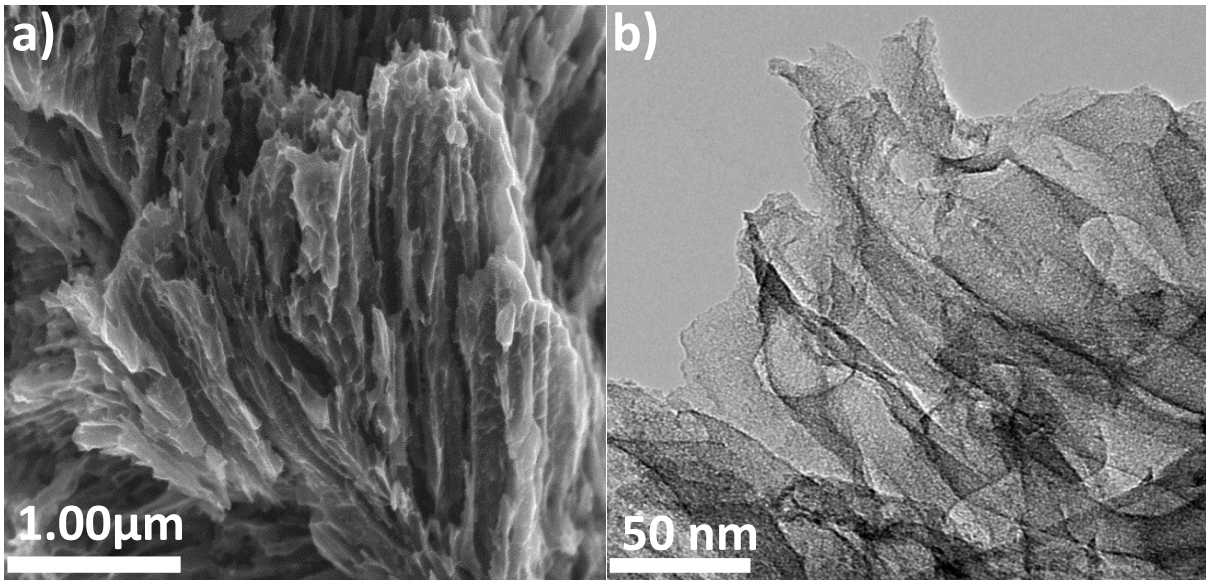

Figure S1. (a, b) SEM and TEM images of N-doped layered mesoporous carbon frameworks.

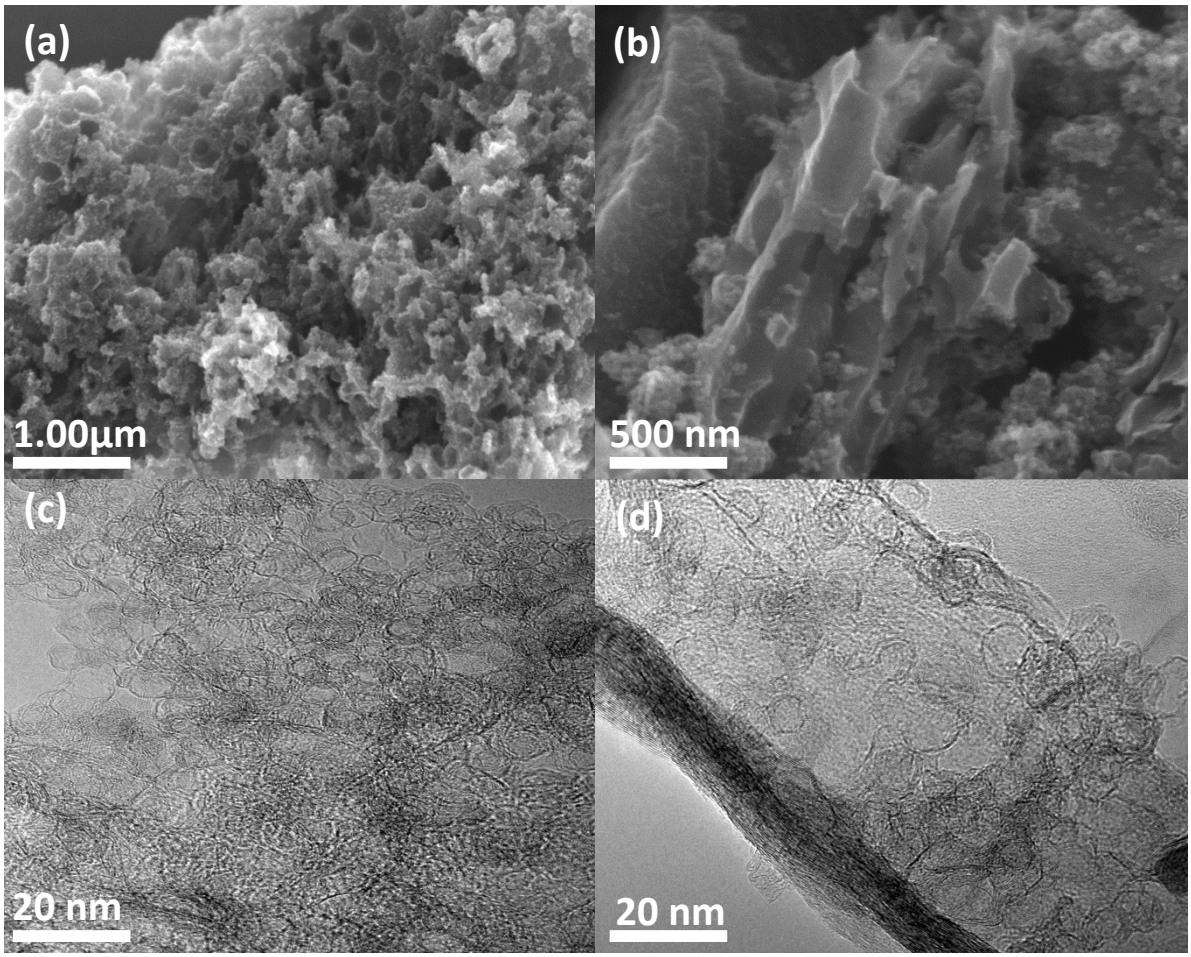

Figure S2. (a,b) SEM images GNNLMCS-21 and GNNLMCS-11. (c, d) TEM images of GNNLMCS-21 and (b,d) GNNLMCS-11.

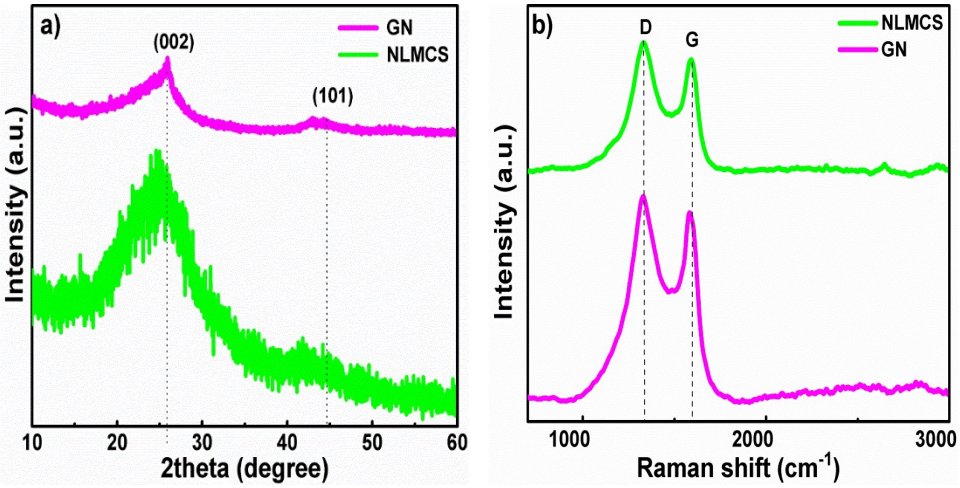

Figure S3. (a) XRD patterns and (b) Raman spectra of GN and NLMCS.

Evidence for non-graphitized and amorphous nature:

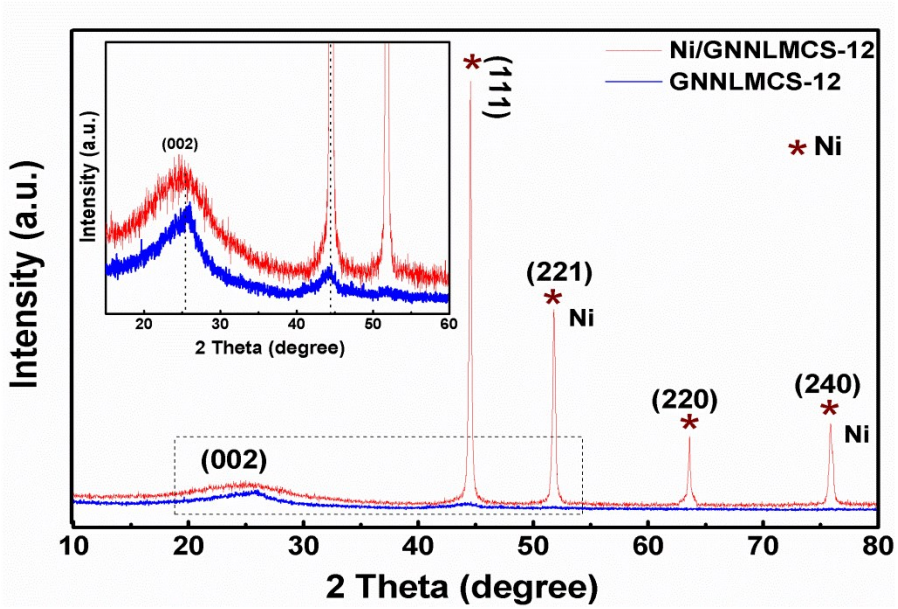

Figure S4. XRD of GNNLMCS-12 before and after acid etching.

Before etching, the XRD pattern of Ni/GNNLMCS-12 shows the XRD diffraction peaks corresponding to graphitic carbon and Ni NPs (around 2θ = 26.2°, 43.4°, 53.3°, 63.1° and 76.6°). In this spectrum, three characteristics peaks of cubic Ni NPs are observed at 53.3°, 63.1° and 76.6° (Fig. S4). After high temperature annealing and acid etching, no other peaks are observed for Ni NPs which confirms that Ni is completely removed from the composite and yielding a highly pure GNNLMCS-12. This GNNLMCS-12 composite shows a diffraction peak at 2θ of about 26.2°, together with a weak broad diffraction peak at about 43.4° in the wide-angle XRD pattern (Fig. S4), suggesting the co-existence of amorphous GN and layered carbons. The XRD patterns for GNNLMCS-11 and GNNLMCS-21 shows indistinct changes, indicating that the GN and NLMCS are successfully self-assembled and make a composite. Typical diffraction patterns for non-graphitized carbon are represented by a characteristic broad 002 diffraction peak at 26.2° and a less intense peak at 43.4°, which corresponds to the 101 reflections. The wide-angle XRD patterns of all of the GNNLMCS materials (Fig. 3a) exhibit two intense peaks which can be indexed as the (002) diffraction and (101) reflection, characteristic of graphitic carbon. The diffraction and reflection peaks for GNNLMCS materials are less intense and well defined in accord with it much lesser graphitized content. The d-spacing of the (002) peak, is a little

larger than that for Ni/GNNLMCS and NLMCS, indicating that the degree of graphitization is limited.

The non-graphitized nature of the GNNLMCS materials is also very evident in the Raman spectra shown in Fig. 3b and Fig. S3b. It is generally accepted that the degree of graphitization (I_D/I_G) specifies the relative amount of defects in graphitic structure and it can be seen that with increase ratio of GN:NLMCS, the I_D/I_G values of GNNLMCS increases gradually from 1.01 to 1.08. The I_D/I_G values for all samples of GNNLMCS, GN and NLMCS are listed in the Table S1. The relative intensity of these D and G lines (ID/IG) depends on the type of graphitic materials and reflects the degree of graphitization[1]. The GNNLMCS materials exhibits a strong and sharp G-band and D-band as well as 2D band with ID/IG=1.01-1.08 in its Raman spectrum, indicating non-graphitized and amorphous nature. The NLMCS composite which was synthesized in the absence of GN have no 2D bands with a low ID/IG of 0.98, indicating only the amorphous nature of the carbon[2]. The observed difference in the Raman spectra for both all mesoporous carbon materials indicates the nature of graphitic carbons synthesized with the addition of GN and NLMCS. Therefore, the XRD and Raman results give evidence for non-graphitized and amorphous carbon frameworks as well as the intercalation of graphene nanospheres into carbon layers.

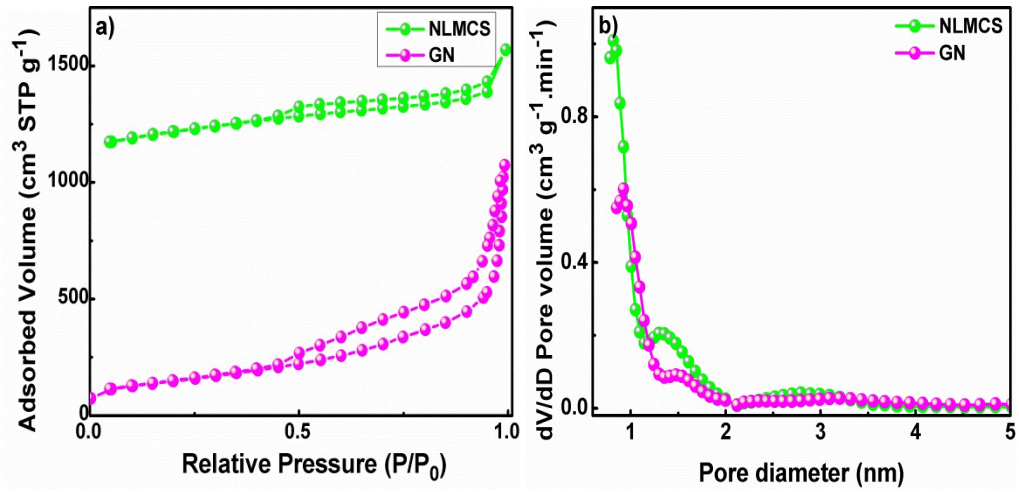

Figure S5. (a) Nitrogen sorption isotherm and (b) pore size distribution profiles of GN and NLMCS.

Table S1. Textural characteristics of the carbon samples.

Electrode materials	S_{BET}[a)] (m^2g^{-1})	V_t[b)] (cm^3g^{-1})	V_{mic}[c)] (cm^3g^{-1})	V_{meso}[d)] (cm^3g^{-1})	Average pore size range (nm)	ID/IG
GNNLMCS-12	1143	0.97	0.39	0.54	0.28-42.31	1.08
GNNLMCS-11	935	0.85	0.42	0.51	0.28-51.22	1.05
GNNLMCS-21	605	1.02	0.72	0.79	0.28-49.34	1.01
NLMCS	554	0.48	0.48	0.43	0.28-45.78	0.98
GN	494	0.41	0.64	0.35	0.26-36.67	1.02

a) Surface area calculated by the BET method; b) Total pore volume; c) Micropore volume; d) Mesopore volume

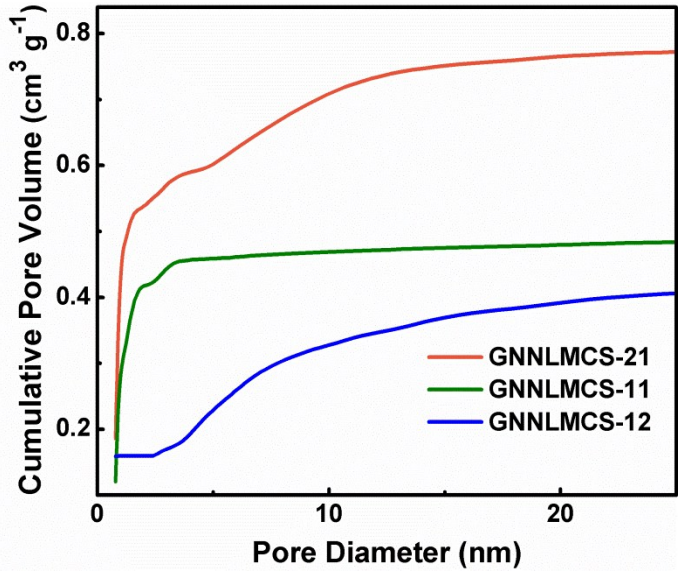

Figure S6. Cumulative pore volume distributions of GNNLMCS frameworks derived from DFT model.

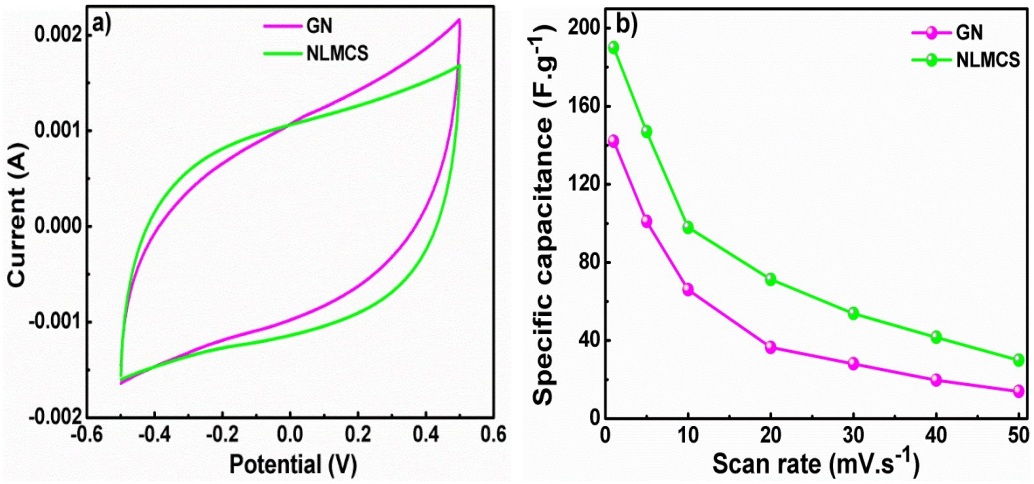

Figure S7. (a) CV curves of GN and NLMCS at a scan rate 1 mV s^{-1} in 0.5 mol L^{-1} NaCl solution. (b) Specific capacitance of GN and NLMCS at different scan rates.

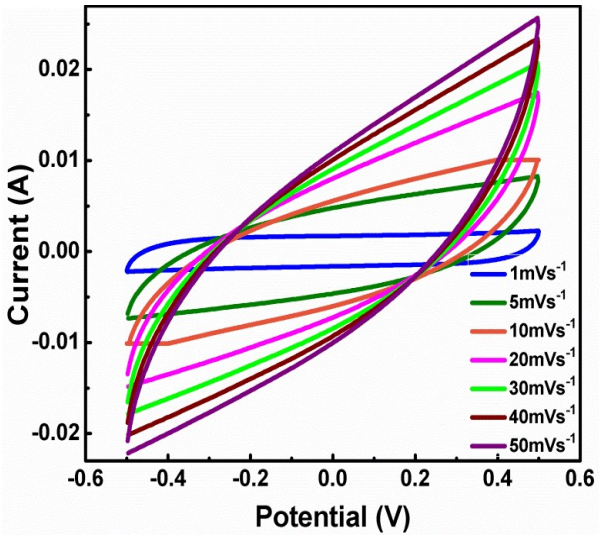

Figure S8. CV curves of GNNLMCS-12 electrode at different scan rate from 1 mV s^{-1} to 50 mV s^{-1} in a 0.5 mol L^{-1} NaCl solution.

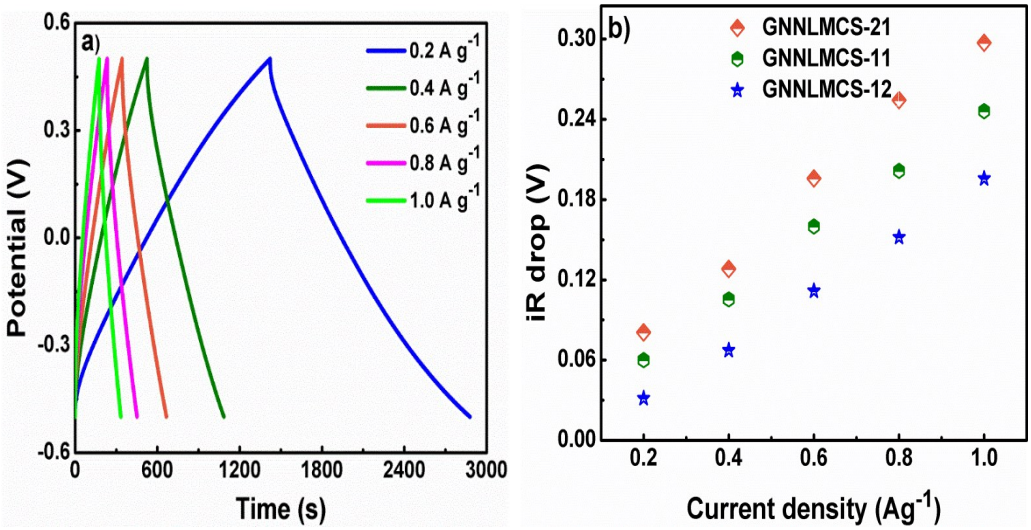

Figure S9. (a) GCD curves of GNNLMCS-12 at various current density in a 0.5 mol L^{-1} NaCl solution. (b) iR drop of GNNLMCS-12, GNNLMCS-11 and GNNLMCS-21 at different discharge current density.

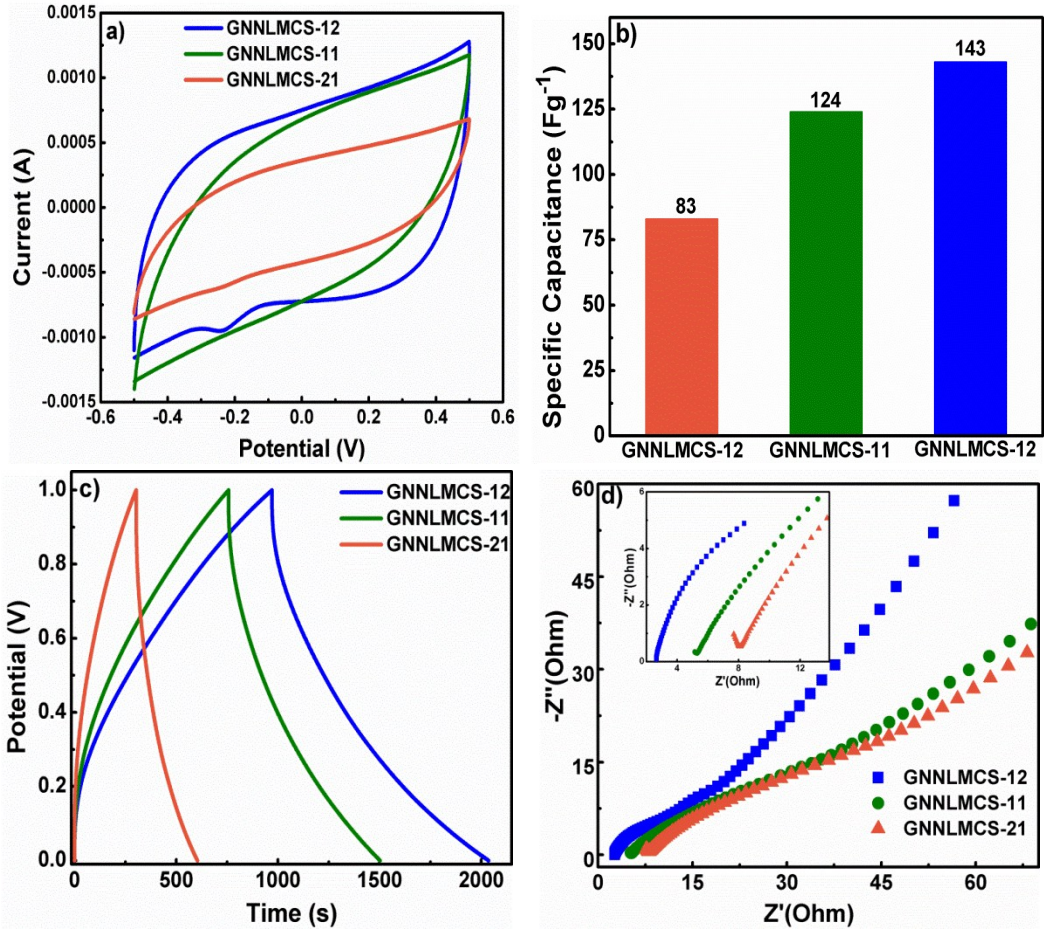

Figure S10. The electrochemical performance of carbon electrodes tested in a 500 ppm NaCl solution. (a) CV curves at 1 mV s^{-1}. (b) The corresponding specific capacitance of the GNNLMCS-12, GNNLMCS-11 and GNNLMCS-21 electrodes at 1 mV s^{-1}. GCD profiles of the carbon electrodes at the current density of 2 A g^{-1}. (d) Nyquist plots of the carbon electrodes.

The electrochemical properties of carbon electrodes tested in a 500 ppm NaCl solution are shown in Figure S10. The CV curves (Figure S10a) of all electrodes displays the distorted shapes even at low scan rate, which should be credited to the sluggish diffusion control process resulting from the low electrolyte concentration. The capacitive current of GNNLMCS-12 is higher than that of other carbon electrodes, suggesting the GNNLMCS-12 possess a better capacitive performance. The corresponding specific capacitances (Cs) are calculated to be 143, 124 and 83 F g^{-1} for the GNNLMCS-12, GNNLMCS-11 and GNNLMCS-21 electrodes, respectively, as shown in Figure S10b. The GCD curves (Figure S10c) of the electrodes also show distorted and unsymmetrical shapes in low electrolyte concentration. The longer charging/discharging time of the GNNLMCS-12 further indicates its better capacitive behavior. The Nyquist plots of all the electrodes are shown in Figure S10d, revealing a much smaller intrinsic ohmic resistance (R_s) of

the GNNLMCS-12 electrode than that of the other electrodes, reflecting that the GNNLMCS-12 electrode has less internal loss and faster charge/discharge rate.

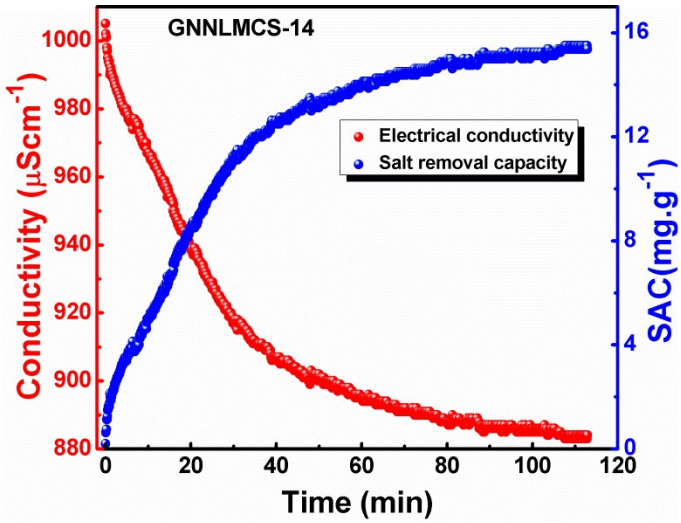

Figure S 11. Plots of solution conductivity and salt removal capacity of GNNLMCS-14 in a 500 mg L^{-1} NaCl solution at 1.2 V with a flow rate of 25 mL min^{-1}.

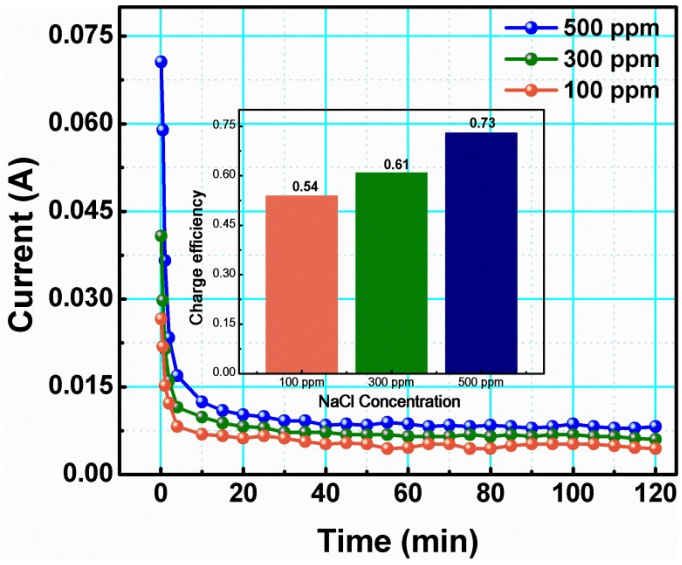

Figure S12. Current response and charge efficiency of GNNLMCS-12 electrode in different concentration of NaCl solution at 1.2 V.

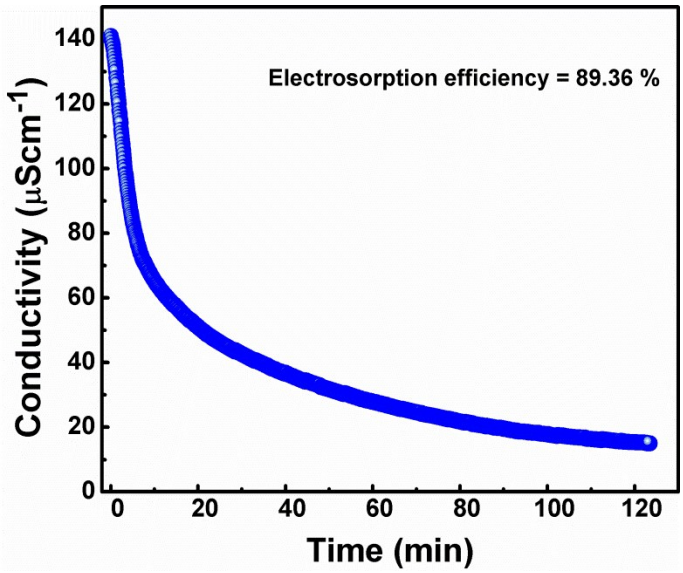

Figure S13. Plots of solution conductivity vs deionization time in a 50 mg L^{-1} NaCl solution at 1.2 V with a flow rate of 25 mL min^{-1}. The electrosorption efficiency of GNNLMCS-12 is around 90 %.

Table S2. Comparison of ion removal capacity of reported carbon materials.

Electrode materials	Initial NaCl concentration [mg L^{-1}]	Applied voltage [V]	Electrodes mass [g]	Ion removal capacity [mg g^{-1}]	Ref.
Activated carbon	500	1.2		9.72	[3]
3D Graphene balls	500	1.2	0.16	12.35	[4]
Carbon aerogel microspheres	500	1.2	0.85	5.62	[5]
N-doped porous carbon sphere	500	1.2	-	13.71	[6]
N-doped porous carbon	500	1.2	0.20	16.63	[7]
Graphene-coated hollow mesoporous carbon spheres	50	1.6	0.50	2.3	[8]
3D Graphene/Metal oxide	500	1.2	0.20	15.5	[9]
Porous graphene frameworks	500	1.4	0.16	19.1	[10]
Porous carbon polyhedra	500	1.2	0.30	13.86	[11]
Mesoporous carbons	250	1.2	0.19	4.8	[12]
GNNLMCS-12	500	1.2	0.16	23.42	This work

References

1. M. Sevilla and A. B. Fuertes, Catalytic graphitization of templated mesoporous carbons, *Carbon*, 2006, **44**, 468-474.
2. Y. Meng, D. Gu, F. Zhang, Y. Shi, L. Cheng, D. Feng, Z. Wu, Z. Chen, Y. Wan and A. Stein, A family of highly ordered mesoporous polymer resin and carbon structures from organic− organic self-assembly, *Chemistry of materials*, 2006, **18**, 4447-4464.
3. Z. Chen, C. Song, X. Sun, H. Guo and G. Zhu, Kinetic and isotherm studies on the electrosorption of NaCl from aqueous solutions by activated carbon electrodes, *Desalination*, 2011, **267**, 239-243.
4. Z. U. Khan, T. Yan, L. Shi and D. Zhang, Improved capacitive deionization by using 3D intercalated graphene sheet–sphere nanocomposite architectures, *Environmental Science: Nano*, 2018, **5**, 980-991.
5. X. Quan, Z. Fu, L. Yuan, M. Zhong, R. Mi, X. Yang, Y. Yi and C. Wang, Capacitive deionization of NaCl solutions with ambient pressure dried carbon aerogel microsphere electrodes, *RSC Advances*, 2017, **7**, 35875-35882.
6. Y. Liu, L. Pan, T. Chen, X. Xu, T. Lu, Z. Sun and D. H. Chua, Porous carbon spheres via microwave-assisted synthesis for capacitive deionization, *Electrochimica Acta*, 2015, **151**, 489-496.
7. Z. Wang, T. Yan, J. Fang, L. Shi and D. Zhang, Nitrogen-doped porous carbon derived from a bimetallic metal–organic framework as highly efficient electrodes for flow-through deionization capacitors, *Journal of Materials Chemistry A*, 2016, **4**, 10858-10868.
8. H. Wang, L. Shi, T. Yan, J. Zhang, Q. Zhong and D. Zhang, Design of graphene-coated hollow mesoporous carbon spheres as high performance electrodes for capacitive deionization, *Journal of Materials Chemistry A*, 2014, **2**, 4739-4750.
9. H. Yin, S. Zhao, J. Wan, H. Tang, L. Chang, L. He, H. Zhao, Y. Gao and Z. Tang, Three-dimensional graphene/metal oxide nanoparticle hybrids for high-performance capacitive deionization of saline water, *Advanced materials*, 2013, **25**, 6270-6276.
10. H. Duan, T. Yan, G. Chen, J. Zhang, L. Shi and D. Zhang, A facile strategy for the fast construction of porous graphene frameworks and their enhanced electrosorption performance, *Chemical Communications*, 2017, **53**, 7465-7468.
11. Y. Liu, X. Xu, M. Wang, T. Lu, Z. Sun and L. Pan, Metal–organic framework-derived porous carbon polyhedra for highly efficient capacitive deionization, *Chemical Communications*, 2015, **51**, 12020-12023.
12. T. Gao, H. Li, F. Zhou, M. Gao, S. Liang and M. Luo, Mesoporous carbon derived from ZIF-8 for high efficient electrosorption, *Desalination*, 2019, **451**, 133-138.